

# Learning to Better Segment Objects from Unseen Classes with Unlabeled Videos

Yuming Du

Yang Xiao

Vincent Lepetit

LIGM, Ecole des Ponts, Univ Gustave Eiffel, CNRS, Marne-la-vallée, France

{yuming.du, yang.xiao, vincent.lepetit}@enpc.fr

<https://dulucas.github.io/Homepage/gbopt/>

## Abstract

The ability to localize and segment objects from unseen classes would open the door to new applications, such as autonomous object learning in active vision. Nonetheless, improving the performance on unseen classes requires additional training data, while manually annotating the objects of the unseen classes can be labor-extensive and expensive. In this paper, we explore the use of unlabeled video sequences to automatically generate training data for objects of unseen classes. It is in principle possible to apply existing video segmentation methods to unlabeled videos and automatically obtain object masks, which can then be used as a training set even for classes with no manual labels available. However, our experiments show that these methods do not perform well enough for this purpose. We therefore introduce a Bayesian method that is specifically designed to automatically create such a training set: Our method starts from a set of object proposals and relies on (non-realistic) analysis-by-synthesis to select the correct ones by performing an efficient optimization over all the frames **simultaneously**. Through extensive experiments, we show that our method can generate a high-quality training set which significantly boosts the performance of segmenting objects of unseen classes. We thus believe that our method could open the door for open-world instance segmentation using abundant Internet videos.

## 1. Introduction

Instance segmentation models are now able to predict the masks of objects of known classes in query images [23, 59, 64], providing rich information for many downstream applications such as scene understanding [21, 56] and robot grasping [62, 69, 72]. Unfortunately, existing instance segmentation methods perform poorly on new classes [15]. This is an obstacle to the development of autonomous systems evolving in open worlds where there will always be

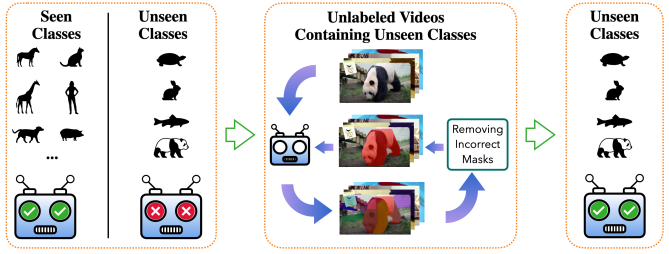


Figure 1. Starting from an instance segmentation model trained on some classes, we want to learn to localize and segment objects from new classes without any human label. We do this by using unlabeled videos, which are an abundant source of data. Our approach can automatically detect and select the object masks in the videos. We then use the selected masks to retrain the initial model that can then localize and segment objects from the new classes in still frames without losing performance on the old ones.

objects that do not belong to known classes. Being able to detect and segment these objects would be the starting point of learning to grasp and manipulate them, for example.

As Figure 1 illustrates, our goal is therefore to automatically improve the performance of instance segmentation models on static images containing objects from new classes without human intervention. This is in contrast with previous works that aiming at limiting the manual labeling burden for object segmentation by using bounding boxes only [26, 34, 77] or developing few-shot techniques [19, 70], but still require human intervention for new classes.

More specifically, we do *not* aim at predicting the categories of these new objects, but focus on robustly localizing and accurately segmenting them. In this sense, our work is therefore more related to recent object discovery methods, which attempt to segment objects without manual segmentation labels by grouping pixels according to some criterion [4, 22, 39, 54, 66]. However, these approaches are still very fragile as they can be easily affected by low-level perturbations in color, lighting, or texture.

Our strategy is therefore to rely on unlabeled video se-

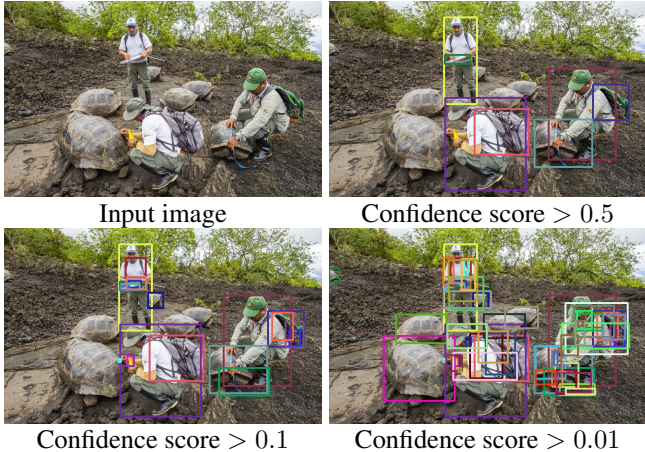


Figure 2. The class ‘tortoise’ does not belong to COCO classes. By decreasing the confidence score threshold of Mask R-CNN [23] trained on COCO, we can eventually localize and segment all the tortoises at the price of introducing many false positives. We filter these false positives using unlabeled video data.

quences, as unlabeled videos can be acquired without effort while providing rich information. The general idea of using videos for self-supervision is not new [13, 28, 36, 40, 63, 65]. Here, we consider video sequences to automatically generate masks for the objects visible in their frames. Using these masks for training an instance segmentation model should then make it perform better on new objects visible in the videos, even if no human intervention was provided in the process. In our experiments, we still provide the videos, but it is possible to imagine a system that captures videos by itself.

Unfortunately, our early experiments showed that state-of-the-art video segmentation methods [18, 41, 50, 36, 60] were not sufficient for this purpose. We therefore developed our own method for automatically creating object masks from videos. Note that our task is subtly different from video segmentation methods, which aim at keeping track of the objects over consecutive frames. For our own goal, this is not needed and we only focus on correctly localizing and segmenting the objects in each frame. Like some video segmentation methods [41], we start from mask hypotheses for the objects visible in the videos obtained with a pre-trained class-agnostic instance segmentation. Such model generalizes to objects from unseen classes to some extent, but at the price of introducing many false positives [49]. Figure 2 shows that when the confidence threshold is lowered, both the detections of objects from unseen classes and incorrect detections get accepted.

It is however possible to filter the incorrect masks using information provided by the videos. Some methods [10, 35, 41, 45, 53] rely on tracklets to track and filter the masks. We claim that such strategy is not optimal, especially for our goal: Image background is underexploited,

while it can be very useful by indicating the *absence* of objects; The optical flow is not used or underexploited, while it gives strong cues about moving objects in videos. To fully exploit the background and motion information across unlabeled video frames, we therefore developed a (non-realistic) analysis-by-synthesis approach. Using a Bayesian framework, we derive an objective function with an additional non-overlapping constraint. The objective function, which consists of three loss terms, is designed to explore the background and motion information to remove incorrect masks and select masks that are temporally consistent over the entire video. The non-overlapping constraint comes from the fact that one pixel can at most belong to one object in the image and helps to reject some false positives. Moreover, we provide a two-stage optimization algorithm to optimize this objective function efficiently.

To evaluate our approach, we created a novel dataset named Unseen-VIS based on the YouTube Video Instance Segmentation (YouTube-VIS) dataset [71], which contains objects that do *not* belong to COCO classes. Starting from the raw masks generated on the training part of Unseen-VIS using a class-agnostic Mask R-CNN pretrained on COCO dataset, we apply our method to automatically select the correct masks. We demonstrate that using these masks can boost the performance of the Mask R-CNN on the test set of Unseen-VIS without losing performance on COCO classes.

To summarize our contributions:

- We propose a Bayesian method to generate high-quality masks on unlabeled videos containing unseen classes;
- We create a benchmark to evaluate the quality of generated masks on unlabeled videos;
- We demonstrate on our benchmark that our proposed method can be used to improve the performance of an instance segmentation model on unseen classes.

## 2. Related Work

In this section, we first review recent works on instance segmentation from color images, especially those targeting new classes. We also review self-learning methods on unlabeled images. Finally, we review several works for video object segmentation as this topic is closely related to our approach.

**Image-level Instance Segmentation.** While state-of-the-art methods for object detection and segmentation [23, 59, 64] rely on large amounts of manually labeled images, a few works aim at reducing the annotation burden for learning to detect and segment object classes. They however still require manual annotations: Weakly-supervised methods require no mask annotations but bounding boxes annotations [26, 34, 77] and few-shot methods require a (small) number of manual object masks [19, 70].

**Self-Learning on Unlabeled Data.** Recently, several methods have been proposed to explore self-supervision using unlabeled static images. They use data distillation [55], unlabeled images from the web [37], consistency across image flipping [29], or an estimate of the uncertainty of prediction [46]. While such approaches are very interesting, unlabelled videos are easily available and have the potential to make the results much more reliable. We compare our method against the most representative methods in our experiments and show we achieve much better performance.

Another type of approach proceeds in a bottom-up fashion by grouping pixels with similar colors or image features to generate masks [4, 22, 39, 54, 66]. However, this can be easily affected by local textures or colors, and some of these methods have been demonstrated on synthetic images only. Because it starts from a pre-trained instance segmentation model, our approach is much more robust.

Like us, some methods leverage unlabeled videos for on urban scene segmentation [8] and face and human detection[30]. However, these works only focus on how to enhance the model performance on the existing classes and do not consider novel classes. [48] makes use of stereo video data together with depth information to reconstruct a static background, then object proposals are generated from the foreground regions by subtraction. While this is an interesting approach, they require depth data and static backgrounds.

**Video Object Segmentation.** Our work also relates to One-Shot, Zero-Shot video object segmentation (VOS) and saliency-based video object segmentation. One-Shot VOS aims at segmenting the objects in the video when the ground truth segmentation is given for a frame. One-Shot VOS methods typically warp the provided segmentation to other frames [5, 36, 63]. They thus require manual annotations and cannot generate new predictions if new objects appear. Some Zero-Shot methods [11, 47, 60, 61] are trained with video labels on seen classes and are able to generalize to unseen classes, but video labeling is very labor-extensive. Some methods look for salient regions in videos [9, 12, 13, 18, 27, 33, 40, 50], as salient regions tend to correspond to objects. However, saliency prediction has two major limitations for our purpose: (a) It can be fooled by non-salient camouflaged objects. (b) Two adjacent objects would be merged into a single salient region, while we want to identify them individually.

Like us, a few methods already adopt a proposal-based approach [3, 41, 45], but rely on classical tracking algorithms to track the proposals such as tracklets. By contrast, our approach relies on (non-realistic) analysis-by-synthesis. Analysis-by-synthesis is an old concept in computer vision, but has been recently increasingly popular. By aiming at explaining the whole image, it can exploit more information.

Moreover, it is conceptually simple and requires few easy-to-fix hyper-parameters. We show in our experiments that our method performs better than the state-of-the-art video object segmentation method UnOVOST [41] for the purpose of generating object masks.

### 3. Method

As discussed in Section 1, our goal is to improve the performance of a pre-trained class-agnostic instance segmentation on unseen classes. Our pipeline consists of three steps:

- **Mask Generation:** We use our baseline instance segmentation network on unlabeled videos containing unseen classes for mask generation;
- **Mask Selection:** We apply our method to automatically select the correct masks on unlabeled videos;
- **Model Refinement:** We use our generated masks to fine-tune or retrain our baseline network to boost its performance on unseen classes.

In this section, we present our baseline instance segmentation network and our approach for automatically selecting high-quality masks by exploring the video information. As we will show in the following section, compared to exhaustive search, our approach is highly efficient and requires few easy-to-fix hyper-parameters.

#### 3.1. Baseline Network for Mask Generation

To generate masks from unlabeled videos, we use a class-agnostic Mask R-CNN [23] with a ResNet-50-FPN [38] backbone as our baseline network. Following previous work [49], we refer to this class-agnostic Mask R-CNN as 'MP R-CNN' for Mask Proposal R-CNN, as it aims only at generating mask proposals regardless of object classes. Note that in practice, Mask R-CNN could be replaced by any other trainable instance segmentation methods. As we mentioned in Section 1, the instance segmentation network may assign low confidence scores for some correct detections of unseen classes. Therefore, during the mask generation stage, we set the confidence score threshold to 0 to get as many detections as possible.

#### 3.2. Mask Selection

Given a video of  $T$  frames, we start from a set of mask candidates  $\mathcal{M}_t = \{M_{t,1}..M_{t,N}\}$  for each frame  $I_t$  obtained using our baseline network, with  $N$  the number of masks candidates in  $I_t$ . To select the mask candidates that actually correspond to objects, we exploit the following cues and constraint:

- The **“Background cue”**: Segmenting typical backgrounds such as sky or grass gives us a cue about where the objects are, whether they move or not.
- The **“Flow cue”**: The optical flow between consecutive frames gives us a cue about the moving objects.

- The “**Consistency cue**”: The selected masks should be consistent not only between consecutive frames, but also over long sequences.
- The “**Non-overlapping constraint**”: An additional constraint that is usually overlooked is that the masks should not overlap: Ideally, one pixel in the image can belong to at most one mask.

As we will show in the following sections, each cue corresponds to a loss term in the final objective function. Each of them and the non-overlapping constraint contribute to removing the false positives, as will be demonstrated by our ablation study in Section 4.3.

To combine these cues to select the correct masks in a given video sequence, we rely on a Bayesian framework. This selection problem can be formalized as maximizing the probability of the detected masks given the frames of the video:

$$P(\mathbf{C}_1, \dots, \mathbf{C}_T | I_1, \dots, I_T), \quad (1)$$

where  $\mathbf{C}_t$  is a set of binary random variables, with  $\mathbf{C}_{t,i} = 1$  corresponding to the event that mask  $M_{t,i}$  is selected and 0 that it is not. We show in the supplementary material that maximizing this probability is equivalent to minimizing the following objective function:

$$\arg \min_{\{\Delta_1, \dots, \Delta_T\}} \sum_t (\lambda_I \mathcal{L}_I(I_t, \Delta_t) + \lambda_F \mathcal{L}_F(F_t, I_t, I_{t+1}, \Delta_t, \Delta_{t+1}) + \lambda_p \mathcal{L}_p(\Delta_t, \Delta_{t+1})), \quad (2)$$

under the non-overlapping constraint that will be detailed below.  $\lambda_I$ ,  $\lambda_F$ , and  $\lambda_p$  are constant weights.  $F_t$  represents the optical flow for the pair of frames  $(I_t, I_{t+1})$ .  $\Delta_t = \{\delta_{t,1}, \dots, \delta_{t,N}\}$  denotes the realization of  $\mathbf{C}_t$  where  $\delta_{t,i}$  is the realization of the random binary variable  $\mathbf{C}_{t,i}$ .  $\delta_{t,i} = 1$  when  $M_{t,i}$  is selected, otherwise  $\delta_{t,i} = 0$ .

We call  $\mathcal{L}_I$  the Background loss and  $\mathcal{L}_F$  the Flow loss, as they exploit the Background cue and the Flow cue respectively.  $\mathcal{L}_p$  enforces consistent selections between consecutive frames. We detail these three losses below.

### 3.2.1 Background Loss $\mathcal{L}_I$

We use  $\mathcal{L}_I$  to exploit the Background cue that hints at where the objects are. As shown in Figure 3, to evaluate it, we compare a binary image generated for the selected masks and the foreground/background probability map predicted by a binary segmentation network  $f$  by calculating their cross entropy, as the image background should match the background of the selected masks. By doing this comparison over all the image locations, we can exploit information from the whole image to guide the mask selection—we will rely on the same strategy for the other terms. Formally, we take

$$\mathcal{L}_I(I_t, \Delta_t) = \text{CE}(\text{Bg}(I_t), 1 - \overline{\text{Fg}}(\Delta_t)), \quad (3)$$

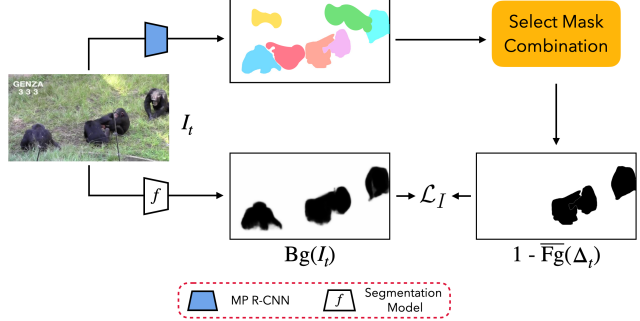


Figure 3. To evaluate the background loss  $\mathcal{L}_I$  of Eq. (3), we compare the background predicted for the image and the background of the selected masks.

where  $\text{CE}$  denotes the cross-entropy,  $\text{Bg}(I_t)$  is a probability map for each pixel to belong to the background as predicted by the network  $f$ , and  $\overline{\text{Fg}}(\Delta_t)$  is the binary image of masks in  $\mathcal{M}_t$  such that  $\delta_{t,i} = 1$ . For  $f$ , we use the network architecture proposed in [32] trained on the same training data as our baseline network for mask generation. The details about the segmentation network  $f$  can be found in the supplementary material.

### 3.2.2 Flow Loss $\mathcal{L}_F$

We use  $\mathcal{L}_F$  to exploit the Flow cue: The optical flow is the result of the object motions and the camera motion, and thus also hints at where the objects are. Even if an object is static but the camera is in motion, when the distance between the camera and the background is large enough, relative motion will make the optical flow of the object regions stand out from the background optical flow.

Figure 4 shows how we evaluate this term. We compare the flow predicted by an optical flow estimator  $g$  and a “synthetic optical flow” generated using the masks selected in  $\mathcal{M}_t$  and  $\mathcal{M}_{t+1}$ . Similar to the  $\mathcal{L}_I$  term, this comparison allows us to exploit information from all the image locations. In practice, we use the method of [58] for  $g$ . To generate the synthetic optical flow, we use the colors of the pixels in the selected masks to compute their optical flow. We average the flow in  $F_t$  on the pixels that do not belong to any mask to assign these pixels the resulting value. The detailed procedure can be found in the supplementary material.

Using this procedure, the measured flow  $F_t = g(I_t, I_{t+1})$  and the synthetic flow are similar when all moving objects are correctly selected in both frames, even when the camera is in motion. More formally, we take:

$$\mathcal{L}_F(F_t, I_t, I_{t+1}, \Delta_t, \Delta_{t+1}) = \|F_t - \overline{F}_t\|_1, \quad (4)$$

where  $\overline{F}_t = \overline{F}_t(I_t, I_{t+1}, \Delta_t, \Delta_{t+1})$  is the synthetic flow generated for the selected masks in  $\mathcal{M}_t$  and  $\mathcal{M}_{t+1}$ . We use the L1-norm to compare the two flows to be robust to outlier

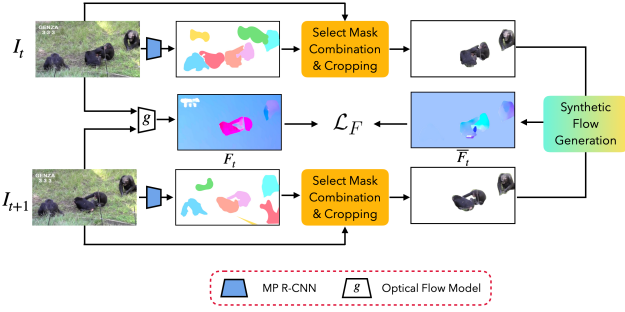


Figure 4. To evaluate the flow loss  $\mathcal{L}_F$  of Eq. (4), we compare the optical flow estimated between two consecutive images and the optical flow computed for the masks selected in the two images.

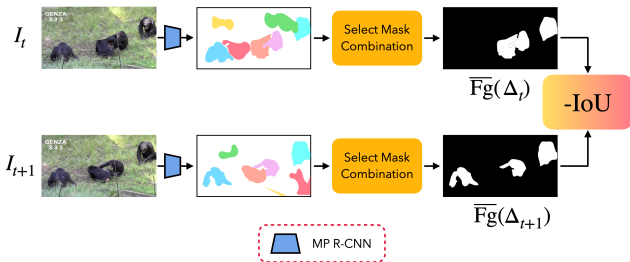


Figure 5. To evaluate the regularization loss  $\mathcal{L}_p$  of Eq. (5), we compare the binary images of the selected masks in two consecutive images.

values that are very common in the predicted flow. Figure 4 shows examples for  $F_t$  and  $\bar{F}_t$ .

### 3.2.3 Regularization Loss $\mathcal{L}_p$ and Constraint

As discussed above, the optimization in Eq. (11) should be done under the constraint that no masks selected for the same frame overlap each other.

$\mathcal{L}_p(\Delta_t, \Delta_{t+1})$  is usually interpreted in tracking problems as a motion model. We use it to enforce a consistent selection of masks between consecutive frames. Figure 5 shows how we compute it: We use a very simple motion model and assume that the objects move slowly, in other words, the areas segmented as objects do not change abruptly between two consecutive frames. Formally, we take :

$$\mathcal{L}_p(\Delta_t, \Delta_{t+1}) = -\text{IoU}(\bar{F}_g(\Delta_t), \bar{F}_g(\Delta_{t+1})), \quad (5)$$

i.e. the negative Intersection-over-Union between the binary images of the masks selected for frames  $I_t$  and  $I_{t+1}$ . It is set to 0 when no masks are selected for none of the two images.

## 3.3. Two-Stage Optimization

In this section, we introduce an efficient way to minimize Eq. (11). Note that minimizing this function requires

to optimize on all the frames simultaneously. A naive approach is to apply exhaustive search for the solution of the problem, where the number of evaluations of the objective function would be  $O(2^{NT})$ , with  $N$  the number of mask candidates per frame and  $T$  the number of frames (typical values  $N = 15$  and  $T = 180$  would require  $\sim 10^{810}$  evaluations). This is clearly computationally prohibitive.

We provide here an efficient two-stage algorithm, depicted in Figure 6. In the first stage, based on the background loss  $\mathcal{L}_I$  and the non-overlapping constraint, we select the top- $K$  most promising combinations of masks for each frame independently. Note that the combinations violating the non-overlapping constraint are simply discarded. Then, in the second stage, we optimize the complete objective function over all frames simultaneously to find the best combinations for each frame. For both stages, we can use Dijkstra's algorithm [16] to significantly decrease the complexity of the computations. In the worst case, the number of evaluations of the objective function becomes  $O(KTN^3 + K^2T^2)$ . We use  $K = 10$  in practice, which reduces the required evaluations from  $\sim 10^{810}$  to  $\sim 10^7$  for the numerical example above.

This optimization problem is related to many previous works on multiple object tracking [2, 42, 53, 68, 73, 74], which typically use graph-based methods to solve related problems efficiently. One of the main differences with these works is that, in our video-level optimization, each node corresponds to a combination of masks instead of a single bounding box or mask. Besides, we do not have access to the object classes, and our optimization is under the constraint that the masks do not overlap, while these works typically rely on bounding boxes that can overlap when the objects are close to each other.

**1. Image-Level Optimization.** At this stage, for each frame  $I_t$ , we look for the top- $K$  combinations of masks in the power set  $\mathcal{P}(\mathcal{M}_t)$  that minimize the Eq.(3) under the non-overlapping constraint. An exhaustive search would take  $2^N$  evaluations of the objective function.

However, we note that this problem can be formulated as a K-shortest path search problem in a binary tree, where each pair of branches of a node corresponds to the selection or not of a mask, and each branch has an associated weight: This weight is set to infinity if the branch corresponds to the selection of a mask that overlaps with one of its ancestors, otherwise it depends on the value of  $\mathcal{L}_I$  computed only on the mask. By iteratively applying Dijkstra's algorithm to find the top- $K$  combinations of masks, we reduce the number of evaluations to  $O(KN^3)$ . Note that our proposed algorithm is agnostic to the order of the mask candidates in  $\mathcal{M}_t$ . More details can be found in the supplementary material.

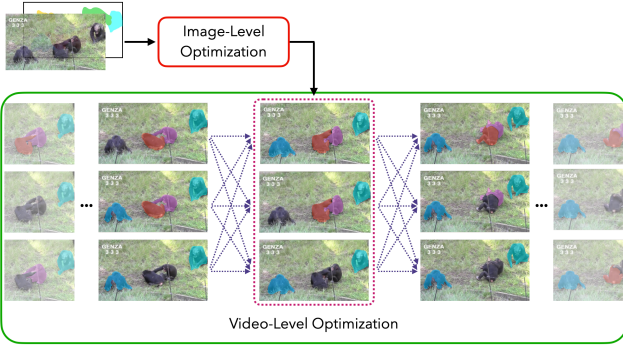


Figure 6. Given a video, we first run the image-level optimisation on each frame and get the top- $K$  combinations of masks for each frame. The video-level optimisation selects the best combination for each frame efficiently by solving a shortest path problem. For this figure,  $K$  is set to 3. More details are given in Section 3.3.

**2. Video-Level Optimization.** As shown in Figure 6, we generate a graph with the remaining top- $K$  combinations of masks for each frame: Each node corresponds to one combination and each edge is labeled with the loss given in Eq.(11) for the two combinations it links. Finding the best combination for each frame becomes the problem of finding the shortest path in this graph. Instead of doing  $2^{KT}$  evaluations of the objective function to find the shortest path, we can use Dijkstra’s algorithm [16] here as well to significantly accelerate the speed of our algorithm. The number of evaluations is reduced to  $O(K^2T^2)$ . We explain in more detail how we build the graph in the supplementary material.

## 4. Experiments

In this section, we first present our benchmark for evaluating our approach. Then we compare our method with several previous methods for the purpose of generating masks on unlabeled videos and analyze the results. We also conduct a thorough ablation study to show the influence of different components of our method. Due to space limits, implementation details were moved to the supplementary material.

### 4.1. Experimental Setup

**Implementation Details.** As described in Section 3.1, we use a class-agnostic Mask R-CNN [23] with a ResNet-50-FPN [38] backbone as our baseline for mask generation. Our baseline is pre-trained on COCO dataset, which contains 80 classes and 115k training images. We follow the training strategy as described in [23]. We take  $\lambda_I = \lambda_F = 1$  and  $\lambda_p = 0.5$  for the weights in Eq. (11) in all our experiments.

**Evaluation.** To benchmark our method, we created a dataset we call “Unseen-VIS”. The training part of

“Unseen-VIS” consists of videos collected from the YouTube Video Instance Segmentation (YouTube VIS) [71] and is used for mask generation. The test part of “Unseen-VIS” contains static images extracted from YouTube VIS for evaluation.

The original YouTube VIS dataset contains 2,883 videos with 131k object instances spanning 40 classes, among which 24 coincide with COCO. We thus consider the remaining 16 classes<sup>1</sup> as *unseen* classes which results in 795 videos in total. We randomly selected 595 videos as the training set, which we refer as Unseen-VIS-train. The labeled static images in the remaining 200 videos are used for evaluation, which we refer as Unseen-VIS-test. All the videos of Unseen-VIS-train are used as unlabeled videos, and their ground truth masks are ignored.

For quantitative evaluation, we rely on the standard COCO metrics:  $AP$ ,  $AP_{50}$ ,  $AP_{75}$ , and  $AR_1$ ,  $AR_3$  and  $AR_5$  as the maximum number of objects per image in our testing set is 4. We do not use  $AP_S$ ,  $AP_M$ , and  $AP_L$  as the object scales in COCO differ largely from YouTube VIS.

## 4.2. Results on Unseen-VIS-test

### 4.2.1 Video-Annotation-Free Mask Generation

We first compare our method to other approaches that can also generate masks given video sequences without using any video annotations. Each method is first applied on the Unseen-VIS-train dataset for mask generation, then we compare the performance of MP R-CNN on the Unseen-VIS-test set after fine-tuning on these masks. As only one over five frames is annotated in Unseen-VIS-train (19352 annotated frames in total), we thus use only the masks of these frames for training for fair comparison among different methods.

**Saliency/Flow-based methods.** FST [50] and NLC [18] can generate masks from videos by estimating the saliency and motion of the objects in videos. IOA [12] trains a deep neural network on the output of an unsupervised soft foreground segmentation algorithm [57] to segment objects in videos. These methods can identify moving regions in the videos but can not separate adjacent objects in the images, thus a proposal generated by these methods may actually correspond to several objects.

**Tracking-based methods.** TWB [3] and UnOVOST [41] rely on a frame-by-frame tracking pipeline applied to mask proposals. These methods are the closest methods to ours as we all rely on an instance segmentation model for proposal generation. However, as we mentioned before, our approach does *not* need to keep track of detected objects.

**Similarity Propagation.** Given a series of masks for one frame, UVC [36] warps these masks to consecutive

<sup>1</sup>panda, lizard, seal, shark, mouse, frog, tiger, leopard, fox, deer, ape, snake, monkey, rabbit, fish, turtle.

Method used for mask generation	Unseen-VIS-test					
	AP	AP <sub>50</sub>	AP <sub>75</sub>	AR <sub>1</sub>	AR <sub>3</sub>	AR <sub>5</sub>
(bef. fine-tuning)	35.8	61.2	38.1	33.3	47.3	50.3
NLC [18]	1.2	3.8	1.0	2.4	5.3	6.9
IOA [12]	2.4	8.5	0.9	6.9	8.7	9.5
FST [50]	17.0	41.8	11.3	22.0	30.6	33.1
UnOVOST [41]	31.1	55.6	32.2	29.9	44.5	48.2
TWB [3]	31.2	53.4	32.8	31.5	46.7	50.0
DD [55]	36.6	63.8	38.5	32.5	46.2	49.3
ZS-UVC [36]	21.2	42.6	19.9	26.3	40.0	43.2
<b>Ours</b>	<b>39.0</b>	<b>67.9</b>	<b>41.3</b>	<b>35.2</b>	<b>48.9</b>	<b>51.4</b>

Table 1. **Mask Generation without Video Annotation.** Performance of MP R-CNN on Unseen-VIS-test after fine-tuning on masks generated by various methods applied to Unseen-VIS-train without using any video annotation.

frames based on the estimated correspondences between consecutive frames. Here, we use it in a zero-shot setting (“ZS-UVC”), where the masks of the first frame are instead generated by thresholding the confidence score on the first frame prediction of MP R-CNN (this threshold is set to 0.1 in practice).

**Self-training methods.** We compare our method with the self-learning Data Distillation (DD) method [55]. We follow their proposed test time augmentation to generate masks on each frame of the Unseen-VIS-train videos independently, as this method performs on single image.

We report the results in Table 1. Compared with the Saliency/Flow-based methods and Tracking-based methods, the masks generated by our method are of high quality and can largely improve the performance of the baseline network in all metrics. Our method also outperforms the state-of-the-art self-training method (DD) [55] for two-stage object detection by a large margin.

#### 4.2.2 Video-Annotation-Dependent Mask Generation

In addition to the aforementioned methods, we further compare with two methods that adopt different settings and explore the upper bound of our method.

**RVOS.** RVOS [60] is an end-to-end video object segmentation framework that directly runs on videos, which requires labeled videos for training. Here, we adopt the Zero-Shot setting for RVOS, where RVOS is trained with ResNet50 [24] as backbone on 1089 videos(25869 annotated frames) of seen classes of YouTube VIS and directly applied to the Unseen-VIS-train videos for mask generation.

**Similarity Propagation.** Here, we consider the One-Shot setting for UVC (“OS-UVC”), where the ground truth masks of the first frame are given for all Unseen-VIS-train videos.

**Selected using GT.** We use the ground truth mask labels of Unseen-VIS-train to select the masks predicted by MP

Method used for mask generation	Video Annotation		Unseen-VIS-test					
	Seen	Unseen	AP	AP <sub>50</sub>	AP <sub>75</sub>	AR <sub>1</sub>	AR <sub>3</sub>	AR <sub>5</sub>
(bef. fine-tuning)			35.8	61.2	38.1	33.3	47.3	50.3
RVOS [60]	✓		38.5	68.9	38.0	35.4	49.5	52.8
Ours		✓	39.0	67.9	41.3	35.2	48.9	51.4
OS-UVC [36]		✓	41.5	73.7	42.9	39.1	52.7	54.9
Selected using GT		✓	42.7	75.1	45.3	37.3	53.4	53.6
Trained with GT	✓		50.8	80.9	54.6	43.6	58.6	60.6

Table 2. **Mask Generation with Video Annotations.** Performance of MP R-CNN on Unseen-VIS-test after fine-tuning on the masks generated by various methods that require manual video annotations except ours. RVOS uses labeled videos of Seen classes for training. OS-UVC uses the ground truth masks for the first frame for mask generation. “Selected using GT” represents the masks generated by MP R-CNN selected using ground truth masks and can be regarded as an upper-bound.

R-CNN. The similarity among masks is evaluated based on their Intersection-over-Union. The Hungarian algorithm is applied during the selection to find the masks that best match with the ground truth. This can be regarded as an upper bound that we can achieve based on only the prediction of MP R-CNN.

**GT.** We report the performance of MP R-CNN fine-tuned with ground truth mask labels of Unseen-VIS-train.

We report the results in Table 2. Compared to RVOS [60] trained with labeled videos, our method can still achieve comparable results on recall while surpassing their results by a large margin on  $AP_{75}$ , which means that the masks selected by our method are of better quality. More importantly, for practical applications, our method was able to deal with the important domain gap between the images in COCO on which we pre-train MP R-CNN and the frames in YouTube VIS on which we apply and evaluate our method. RVOS was trained and applied on videos from YouTube VIS, and therefore was not confronted to a domain gap.

While OS-UVC [36] achieves higher results than our approach, it relies mainly on a high-quality first frame mask: We observe a large performance drop when we replace the ground truth masks (“OS-UVC” in Table 2) by the predicted masks (“ZS-UVC” in Table 1). Besides, it can only track objects appearing in the first frame while unable to handle the emergence of disappearance of objects.

After simply retraining from scratch both on the 80 seen classes of COCO and the masks generated by our approach on Unseen-VIS-train, MP R-CNN achieves 35.2 mask AP on COCO minival and 38.9 mask AP on Unseen-VIS-test. Compared with the MP R-CNN pre-trained only with COCO dataset, which achieves 35.3 mask AP on COCO minival, we manage to achieve better performance on Unseen-VIS-test while maintaining the performance on COCO. More details can be found in the supplementary material.

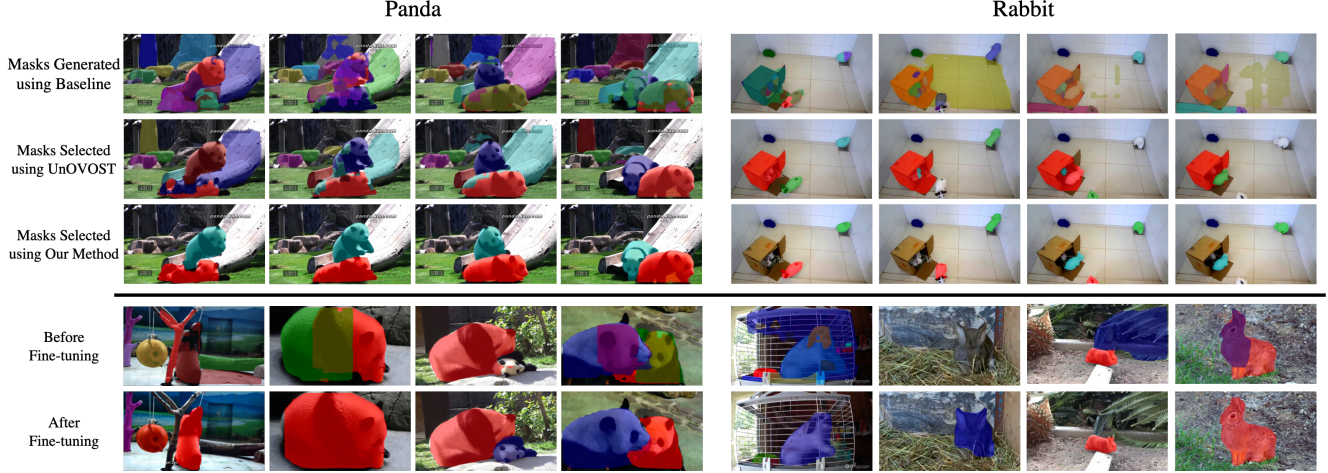


Figure 7. **Qualitative results of selected masks and detections of new classes after fine-tuning.** **Top:** Masks extracted from a sequence from Unseen-VIS-train. First row: Masks detected by our baseline network MP R-CNN; Second row: Masks selected by UnOVOST [41]; Third row: Masks selected by our approach. **Bottom:** Masks detected in still images from Unseen-VIS-test. Fourth row: The MP R-CNN before fine-tuning on our selected masks; Fifth row: the MP R-CNN after fine-tuning on our selected masks. The masks generated by our method results in a significantly better model for the new classes. *For more examples, please refer to the video in the supplementary material.*

Method	Use Unla-beled Data			$\mathcal{J}$ & $\mathcal{F}$			$\mathcal{F}$		
	Mean	Mean	Recall	Mean	Recall	Decay	Mean	Recall	Decay
UnOVOST [41]		56.2	54.4	63.7	-0.01		57.9	65.0	0.00
UnOVOST+	✓	<b>59.9</b>	<b>59.1</b>	<b>70.0</b>	<b>-0.06</b>		<b>60.8</b>	<b>70.8</b>	<b>-0.03</b>

Table 3. **Zero-Shot Video Object Segmentation evaluation on the DAVIS dataset [52].** UnOVOST [41] relies on an instance segmentation network for mask generation. UnOVOST+ row: After fine-tuning its mask generation network on the DAVIS training dataset using the masks generated by our approach, it achieves higher results on all metrics.

**Application to Zero-Shot Video Object Segmentation.** As one of the state-of-the-art zero-shot video object segmentation methods<sup>2</sup>, UnOVOST [41] segments the objects in the videos by linking the masks predicted by an instance segmentation network on each frame. As shown in Table 3, by fine-tuning the original mask generation model on the masks generated on the DAVIS training dataset [52] using our method, we achieve much better results. This demonstrates that downstream tasks can benefit from the performance boost brought by our method.

### 4.3. Ablation Study

Table 4 shows the positive impact made by each loss term and constraint in Eq. (11). The masks obtained by applying only the background loss  $\mathcal{L}_I$  can already improve the performance of baseline on unseen classes. Similarly, adding the constraint that the masks should not overlap, the flow loss  $\mathcal{L}_F$ , or the regularization loss  $\mathcal{L}_p$  has a positive impact. In particular, this shows that both the flow loss  $\mathcal{L}_F$  and the regularization loss  $\mathcal{L}_p$  help reranking the combinations of masks given by the background loss.

$\mathcal{L}_I$	Constraint	$\mathcal{L}_F$	$\mathcal{L}_p$	AP	AP <sub>50</sub>	AP <sub>75</sub>	AR <sub>1</sub>	AR <sub>3</sub>	AR <sub>5</sub>
				35.8	61.2	38.1	33.3	47.3	50.3
✓				36.6	65.2	37.8	33.3	47.7	50.8
✓	✓			38.1	64.6	40.2	34.2	48.5	51.2
✓	✓	✓		38.7	67.0	40.5	34.7	48.7	51.3
✓	✓	✓	✓	39.0	67.9	41.3	35.2	48.9	51.4

Table 4. **Ablation study** on the different components of our method.

## 5. Conclusion

In this paper, we attacked the problem of localizing and segmenting objects from unseen classes without any manual mask labels. We showed that, based on an instance segmentation model pretrained on some seen classes, our method provides high-quality masks for unseen classes after analysing unlabeled videos, without requiring difficult-to-tune hyper-parameters. Moreover, we provided an efficient implementation by breaking down the computationally prohibitive optimization into a two-stage optimization.

It should nevertheless be noted that, in the unsupervised case, the concept of objects is quite ill-defined. The boundary between “things” and “stuff” [6, 20] is sometimes fuzzy: For example, should we consider a stone on the background as an object? What if a person pushes this stone? The granularity of the problem is also not clear: Should we consider a person as one object, or each of their clothes as individual objects? This ambiguity does not arise in the supervised case, as the annotators decide what is an object, but makes the evaluation of unsupervised object detection difficult. It may be important to rethink the definition of object, either by its shape or its function, to make the evaluation of unsupervised object segmentation more meaningful.

<sup>2</sup><https://davischallenge.org/challenge2019/leaderboards.html>

## References

- [1] Radhakrishna Achanta, Appu Shaji, Kevin Smith, Aurelien Lucchi, Pascal Fua, and Sabine Süstrunk. SLIC Superpixels Compared to State-Of-The-Art Superpixel Methods. *IEEE TPAMI*, 34(11), 2012.
- [2] Jérôme Berclaz, Francois Fleuret, Engin Turetken, and Pascal Fua. Multiple Object Tracking Using K-Shortest Paths Optimization. *IEEE TPAMI*, 33(9), 2011.
- [3] Philipp Bergmann, Tim Meinhardt, and Laura Leal-Taixé. Tracking Without Bells and Whistles. In *CVPR*, 2019.
- [4] Christopher P. Burgess, Loic Matthey, Nicholas Watters, Rishabh Kabra, Irina Higgins, Matt Botvinick, and Alexander Lerchner. Monet: Unsupervised Scene Decomposition and Representation. In *arXiv*, 2019.
- [5] Sergi Caelles, Kevis-Kokitsi Maninis, Jordi Pont-Tuset, Laura Leal-Taixé, Daniel Cremers, and Luc Van Gool. One-Shot Video Object Segmentation. In *CVPR*, 2017.
- [6] Holger Caesar, Jasper Uijlings, and Vittorio Ferrari. COCO-Stuff: Thing and Stuff Classes in Context. In *CVPR*, 2018.
- [7] Angel X. Chang, Thomas Funkhouser, Leonidas Guibas, Pat Hanrahan, Qixing Huang, Zimo Li, Silvio Savarese, Manolis Savva, Shuran Song, Hao Su, and Others. Shapenet: An Information-Rich 3D Model Repository. In *arXiv*, 2015.
- [8] Liang-Chieh Chen, Raphael Gontijo Lopes, Bowen Cheng, Maxwell D. Collins, Ekin D. Cubuk, Barret Zoph, Hartwig Adam, and Jonathon Shlens. Naive-Student: Leveraging Semi-Supervised Learning in Video Sequences for Urban Scene Segmentation. In *ECCV*, 2020.
- [9] Yi-Wen Chen, Yi-Hsuan Tsai, Yen-Yu Lin, and Ming-Hsuan Yang. VOSTR: Video Object Segmentation via Transferable Representations. *IJCV*, 128(4), 2020.
- [10] Jingchun Cheng, Yi-Hsuan Tsai, Wei-Chih Hung, Shengjin Wang, and Ming-Hsuan Yang. Fast and Accurate Online Video Object Segmentation via Tracking Parts. In *CVPR*, 2018.
- [11] Jingchun Cheng, Yi-Hsuan Tsai, Shengjin Wang, and Ming-Hsuan Yang. SegFlow: Joint Learning for Video Object Segmentation and Optical Flow. In *ICCV*, 2017.
- [12] Ioana Croitoru, Simion-Vlad Bogolin, and Marius Leordeanu. Unsupervised Learning from Video to Detect Foreground Objects in Single Images. In *ICCV*, 2017.
- [13] Achal Dave, Pavel Tokmakov, and Deva Ramanan. Towards Segmenting Anything That Moves. In *ICCV*, 2019.
- [14] Jia Deng, Wei Dong, Richard Socher, Li-Jia Li, Kai Li, and Li Fei-Fei. ImageNet: A Large-Scale Hierarchical Image Database. In *CVPR*, 2009.
- [15] Akshay Dhamija, Manuel Gunther, Jonathan Ventura, and Terrance Boult. The Overlooked Elephant of Object Detection: Open Set. In *WACV*, 2020.
- [16] Edsger W. Dijkstra. A Note on Two Problems in Connexion with Graphs. *Numerische mathematik*, 1(1), 1959.
- [17] Piotr Dollár and C. Lawrence Zitnick. Structured Forests for Fast Edge Detection. In *ICCV*, 2013.
- [18] Alon Faktor and Michal Irani. Video Segmentation by Non-Local Consensus Voting. In *BMVC*, 2014.
- [19] Zhibo Fan, Jin-Gang Yu, Zhihao Liang, Jiarong Ou, Changxin Gao, G. Xia, and Y. Li. FGN: Fully Guided Network for Few-Shot Instance Segmentation. In *CVPR*, 2020.
- [20] D. A. Forsyth, J. Malik, M. M. Fleck, H. Greenspan, T. K. Leung, S. Belongie, C. Carson, and C. Bregler. Finding Pictures of Objects in Large Collections of Images. In *Object Representation in Computer Vision*, 1996.
- [21] Georgia Gkioxari, Jitendra Malik, and Justin Johnson. Mesh R-CNN. In *ICCV*, 2019.
- [22] Klaus Greff, Raphaël Lopez Kaufman, Rishabh Kabra, Nick Watters, Christopher Burgess, Daniel Zoran, Loic Matthey, Matthew Botvinick, and Alexander Lerchner. Multi-Object Representation Learning with Iterative Variational Inference. In *ICML*, 2019.
- [23] Kaiming He, Georgia Gkioxari, Piotr Dollár, and Ross Girshick. Mask R-CNN. In *ICCV*, 2017.
- [24] Kaiming He, Xiangyu Zhang, Shaoqing Ren, and Jian Sun. Deep Residual Learning for Image Recognition. In *CVPR*, 2016.
- [25] Geoffrey E. Hinton. Products of Experts. In *International Conference on Artificial Neural Networks*, 1999.
- [26] Ronghang Hu, Piotr Dollár, Kaiming He, Trevor Darrell, and Ross Girshick. Learning to Segment Every Thing. In *CVPR*, 2018.
- [27] Suyog Dutt Jain, Bo Xiong, and Kristen Grauman. Fusionseg: Learning to Combine Motion and Appearance for Fully Automatic Segmentation of Generic Objects in Videos. In *CVPR*, 2017.
- [28] Tomas Jakab, Ankush Gupta, Hakan Bilen, and Andrea Vedaldi. Self-Supervised Learning of Interpretable Keypoints from Unlabelled Videos. In *CVPR*, 2020.
- [29] Jisoo Jeong, Seungeui Lee, Jeesoo Kim, and Nojun Kwak. Consistency-Based Semi-Supervised Learning for Object Detection. In *NeurIPS*, 2019.
- [30] SouYoung Jin, Aruni Roychowdhury, Huaizu Jiang, Ashish Singh, Aditya Prasad, Deep Chakraborty, and Erik Learned-Miller. Unsupervised Hard Example Mining from Videos for Improved Object Detection. In *ECCV*, 2018.
- [31] Will Kay, Joao Carreira, Karen Simonyan, Brian Zhang, Chloe Hillier, Sudheendra Vijayanarasimhan, Fabio Viola, Tim Green, Trevor Back, Paul Natsev, and Others. The Kinetics Human Action Video Dataset. In *arXiv*, 2017.
- [32] Alexander Kirillov, Kaiming He, Ross Girshick, Carsten Rother, and Piotr Dollár. Panoptic Segmentation. In *CVPR*, 2019.
- [33] Yeong Jun Koh and Chang-Su Kim. Primary Object Segmentation in Videos Based on Region Augmentation and Reduction. In *CVPR*, 2017.
- [34] Weicheng Kuo, A. Angelova, Jitendra Malik, and Tsung-Yi Lin. ShapeMask: Learning to Segment Novel Objects by Refining Shape Priors. In *ICCV*, 2019.
- [35] Fuxin Li, Taeyoung Kim, Ahmad Humayun, David Tsai, and James M. Rehg. Video Segmentation by Tracking Many Figure-Ground Segments. In *ICCV*, 2013.
- [36] Xueting Li, Sifei Liu, Shalini De mello, Xiaolong Wang, Jan Kautz, and Ming-Hsuan Yang. Joint-Task Self-Supervised Learning for Temporal Correspondence. In *NeurIPS*, 2019.

[37] Yandong Li, Di Huang, Danfeng Qin, Liqiang Wang, and Boqing Gong. Improving Object Detection with Selective Self-Supervised Self-Training. In *ECCV*, 2020.

[38] Tsung-Yi Lin, Piotr Dollár, Ross Girshick, Kaiming He, Bharath Hariharan, and Serge Belongie. Feature Pyramid Networks for Object Detection. In *CVPR*, 2017.

[39] Francesco Locatello, Dirk Weissenborn, Thomas Unterthiner, Aravindh Mahendran, Georg Heigold, Jakob Uszkoreit, Alexey Dosovitskiy, and Thomas Kipf. Object-Centric Learning with Slot Attention. In *NeurIPS*, 2020.

[40] Xiankai Lu, Wenguan Wang, Jianbing Shen, Yu-Wing Tai, David J. Crandall, and Steven C.H. Hoi. Learning Video Object Segmentation from Unlabeled Videos. In *CVPR*, 2020.

[41] Jonathon Luiten, Idil Esen Zulfikar, and Bastian Leibe. Un-OVOST: Unsupervised Offline Video Object Segmentation and Tracking. In *WACV*, 2020.

[42] Tianyang Ma and Longin Jan Latecki. Maximum Weight Cliques with Mutex Constraints for Video Object Segmentation. In *CVPR*, 2012.

[43] Francisco Massa and Ross Girshick. Maskrcnn-Benchmark: Fast, Modular Reference Implementation of Instance Segmentation and Object Detection Algorithms in PyTorch. <https://github.com/facebookresearch/maskrcnn-benchmark>, 2018.

[44] N. Mayer, E. Ilg, P. Häusser, P. Fischer, D. Cremers, A. Dosovitskiy, and T. Brox. A Large Dataset to Train Convolutional Networks for Disparity, Optical Flow, and Scene Flow Estimation. In *ICCV*, 2016.

[45] Anton Milan, Laura Leal-Taixé, Konrad Schindler, and Ian Reid. Joint Tracking and Segmentation of Multiple Targets. In *CVPR*, 2015.

[46] Natalia Neverova, David Novotny, and Andrea Vedaldi. Correlated Uncertainty for Learning Dense Correspondences from Noisy Labels. In *NeurIPS*, 2019.

[47] Seoung Wug Oh, Joon-Young Lee, Ning Xu, and Seon Joo Kim. Video Object Segmentation Using Space-Time Memory Networks. In *ICCV*, 2019.

[48] Aljoša Ošep, Paul Voigtlaender, Jonathon Luiten, Stefan Breuers, and Bastian Leibe. Large-Scale Object Mining for Object Discovery from Unlabeled Video. In *ICRA*, 2019.

[49] Aljoša Ošep, Paul Voigtlaender, Mark Weber, Jonathon Luiten, and Bastian Leibe. 4D Generic Video Object Proposals. In *ICRA*, 2020.

[50] Anestis Papazoglou and Vittorio Ferrari. Fast Object Segmentation in Unconstrained Video. In *ICCV*, 2013.

[51] Deepak Pathak, Ross Girshick, Piotr Dollár, Trevor Darrell, and Bharath Hariharan. Learning Features by Watching Objects Move. In *CVPR*, 2017.

[52] Federico Perazzi, Jordi Pont-Tuset, Brian McWilliams, Luc Van Gool, Markus Gross, and Alexander Sorkine-Hornung. A Benchmark Dataset and Evaluation Methodology for Video Object Segmentation. In *CVPR*, 2016.

[53] Federico Perazzi, Oliver Wang, Markus Gross, and Alexander Sorkine-Hornung. Fully Connected Object Proposals for Video Segmentation. In *ICCV*, 2015.

[54] Trung Pham, Vijay BG Kumar, Thanh-Toan Do, Gustavo Carneiro, and Ian Reid. Bayesian Semantic Instance Segmentation in Open Set World. In *ECCV*, 2018.

[55] Ilija Radosavovic, P. Dollár, Ross B. Girshick, Georgia Gkioxari, and Kaiming He. Data Distillation: Towards Omni-Supervised Learning. In *CVPR*, 2018.

[56] Martin Runz, Kejie Li, Meng Tang, Lingni Ma, Chen Kong, Tanner Schmidt, Ian Reid, Lourdes Agapito, Julian Straub, Steven Lovegrove, and Richard Newcombe. FroDO: From Detections to 3D Objects. In *CVPR*, 2020.

[57] Otilia Stretcu and Marius Leordeanu. Multiple Frames Matching for Object Discovery in Video. In *BMVC*, 2015.

[58] Zachary Teed and Jia Deng. RAFT: Recurrent All-Pairs Field Transforms for Optical Flow. In *ECCV*, 2020.

[59] Zhi Tian, Chunhua Shen, and Hao Chen. Conditional Convolutions for Instance Segmentation. In *ECCV*, 2020.

[60] Carles Ventura, Miriam Bellver, Andreu Girbau, Amaia Salvador, Ferran Marques, and Xavier Giro-I-Nieto. RVOS: End-To-End Recurrent Network for Video Object Segmentation. In *CVPR*, 2019.

[61] Paul Voigtlaender, Yuning Chai, Florian Schroff, Hartwig Adam, Bastian Leibe, and Liang-Chieh Chen. FEELVOS: Fast End-To-End Embedding Learning for Video Object Segmentation. In *CVPR*, 2019.

[62] Kentaro Wada, Kei Okada, and Masayuki Inaba. Joint Learning of Instance and Semantic Segmentation for Robotic Pick-and-Place with Heavy Occlusions in Clutter. In *ICRA*, 2019.

[63] Xiaolong Wang, Allan Jabri, and Alexei A. Efros. Learning Correspondence from the Cycle-Consistency of Time. In *CVPR*, 2019.

[64] Xinlong Wang, Tao Kong, Chunhua Shen, Yuning Jiang, and Lei Li. SOLO: Segmenting Objects by Locations. In *ECCV*, 2020.

[65] Nicholas Watters, Daniel Zoran, Theophane Weber, Peter Battaglia, Razvan Pascanu, and Andrea Tacchetti. Visual Interaction Networks: Learning a Physics Simulator from Video. In *NeurIPS*, 2017.

[66] Kelvin Wong, Shenlong Wang, Mengye Ren, Ming Liang, and Raquel Urtasun. Identifying Unknown Instances for Autonomous Driving. In *Conference on Robot Learning*, 2020.

[67] Yuxin Wu, Alexander Kirillov, Francisco Massa, Wan-Yen Lo, and Ross Girshick. Detectron2. <https://github.com/facebookresearch/detectron2>, 2019.

[68] Zheng Wu, Thomas H. Kunz, and Margrit Betke. Efficient Track Linking Methods for Track Graphs Using Network-Flow and Set-Cover Techniques. In *CVPR*, 2011.

[69] Christopher Xie, Yu Xiang, Arsalan Mousavian, and Dieter Fox. The Best of Both Modes: Separately Leveraging RGB and Depth for Unseen Object Instance Segmentation. In *Conference on robot learning*, 2020.

[70] Xiaopeng Yan, Ziliang Chen, Anni Xu, Xiaoxi Wang, Xiaodan Liang, and L. Lin. Meta R-CNN: Towards General Solver for Instance-Level Low-Shot Learning. In *ICCV*, 2019.

[71] Linjie Yang, Yuchen Fan, and Ning Xu. Video Instance Segmentation. In *ICCV*, 2019.

[72] Lin Yen-Chen, Andy Zeng, Shuran Song, Phillip Isola, and Tsung-Yi Lin. Learning to See Before Learning to Act: Visual Pre-Training for Manipulation. In *ICRA*, 2020.

- [73] Amir Roshan Zamir, Afshin Dehghan, and Mubarak Shah. GMCP-Tracker: Global Multi-Object Tracking Using Generalized Minimum Clique Graphs. In *ECCV*, 2012.
- [74] Dong Zhang, Omar Javed, and Mubarak Shah. Video Object Segmentation through Spatially Accurate and Temporally Dense Extraction of Primary Object Regions. In *CVPR*, 2013.
- [75] Hang Zhang, Chongruo Wu, Zhongyue Zhang, Yi Zhu, Zhi Zhang, Haibin Lin, Yue Sun, Tong He, Jonas Mueller, R. Manmatha, and Others. Resnest: Split-Attention Networks. In *arXiv*, 2020.
- [76] Hengshuang Zhao, Jianping Shi, Xiaojuan Qi, Xiaogang Wang, and Jiaya Jia. Pyramid Scene Parsing Network. In *CVPR*, 2017.
- [77] Yanzhao Zhou, Xin Wang, Jianbin Jiao, and Trevor Darrell. Learning Saliency Propagation for Semi-Supervised Instance Segmentation. In *CVPR*, 2020.

## A. Formulation

As discussed in Section 1 of the main paper, our goal is to improve the performance of a pre-trained class-agnostic instance segmentation on unseen classes. We do this by first using this model for mask generation on unlabeled video sequences. Then we apply our method to automatically select the correct masks and use them to train the instance segmentation model and boost its performance on unseen classes.

Given a video of  $T$  frames, we start from a set of mask candidates  $\mathcal{M}_t = \{M_{t,1}..M_{t,N}\}$  for each frame  $I_t$  obtained using a pre-trained class-agnostic instance segmentation model, with  $N$  the number of masks candidates in  $I_t$ . To select the mask candidates that actually correspond to objects, we want to exploit several cues and a constraint:

- The “**Background cue**”: Segmenting typical backgrounds such as sky or grass gives us a cue about where the objects are, whether they move or not.
- The “**Flow cue**”: The optical flow between consecutive frames gives us a cue about the moving objects.
- The “**Consistency cue**”: The selected masks should be consistent not only between consecutive frames, but also over long sequences.
- The “**Non-overlapping constraint**”: An additional constraint that is usually overlooked is that the masks should not overlap: Ideally, one pixel in the image can belong to at most one mask.

To combine these cues to select the correct masks, we rely on a Bayesian framework. The selection problem can be formalized as maximizing:

$$P(\mathbf{C}_1, \dots, \mathbf{C}_T | I_1, \dots, I_T), \quad (6)$$

where  $\mathbf{C}_t$  is a set of binary random variables, with  $\mathbf{C}_{t,i} = 1$  corresponding to the event that the mask  $M_{t,i}$  is selected and 0 that it is not. By applying Bayes’ theorem, the problem becomes the maximization of:

$$P(I_1, \dots, I_T | \mathbf{C}_1, \dots, \mathbf{C}_T) P(\mathbf{C}_1, \dots, \mathbf{C}_T). \quad (7)$$

To keep both the image and optical flow cues, we use a Product-of-Experts [25] with cliques made of two consecutive images to model the first term as:

$$P(I_1, \dots, I_T | \mathbf{C}_1, \dots, \mathbf{C}_T) \propto \prod_t P(I_t, I_{t+1} | \mathbf{C}_1, \dots, \mathbf{C}_T). \quad (8)$$

We make the standard assumptions that the successive states (the  $\mathbf{C}_t$ ) follow a Markov process, and that the measurements at time  $t$  (the  $I_t$ ) depend only upon the current state ( $\mathbf{C}_t$ ). We denote  $\delta_{t,i}$  the realization of the random binary variable  $\mathbf{C}_{t,i}$  (thus  $\delta_{t,i} \in \{0, 1\}$ ) and  $\Delta_t = \{\delta_{t,1}, \dots, \delta_{t,N}\}$

the realization of  $\mathbf{C}_t$ . After standard derivations, the optimization problem becomes:

$$\arg \max_{\{\Delta_1, \dots, \Delta_T\}} \prod_t P(I_t, I_{t+1} | \mathbf{C}_t, \mathbf{C}_{t+1}) P(\mathbf{C}_{t+1} | \mathbf{C}_t). \quad (9)$$

$P(I_t, I_{t+1} | \mathbf{C}_t, \mathbf{C}_{t+1})$  is high when the image likelihoods  $P(I_t | \mathbf{C}_t)$  and  $P(I_{t+1} | \mathbf{C}_{t+1})$  are high and when the object motions between  $I_t$  and  $I_{t+1}$  are consistent with states  $\mathbf{C}_t$  and  $\mathbf{C}_{t+1}$ .  $P(I_t, I_{t+1} | \mathbf{C}_t, \mathbf{C}_{t+1})$  is thus directly proportional to:

$$P(I_t | \mathbf{C}_t) P(I_{t+1} | \mathbf{C}_{t+1}) P(F_t | I_t, I_{t+1}, \mathbf{C}_t, \mathbf{C}_{t+1}), \quad (10)$$

where  $F_t$  is the optical flow for the pair of frames  $(I_t, I_{t+1})$ . After taking the log of Eq. (9), the optimization problem can be written as:

$$\arg \min_{\{\Delta_1, \dots, \Delta_T\}} \sum_t \lambda_I \mathcal{L}_I(I_t, \Delta_t) + \lambda_F \mathcal{L}_F(F_t, I_t, I_{t+1}, \Delta_t, \Delta_{t+1}) + \lambda_p \mathcal{L}_p(\Delta_t, \Delta_{t+1}), \quad (11)$$

under the non-overlapping constraint.  $\lambda_I$ ,  $\lambda_F$ , and  $\lambda_p$  are weights. We take  $\lambda_I = \lambda_F = 1$  and  $\lambda_p = 0.5$  in all our experiments.

## B. Two-Stage Optimization

In this section, we detail our efficient two-stage optimization of the objective function in Eq. 11. Recall that, in the first stage, we select the most promising combinations of masks for each frame independently using the background loss  $\mathcal{L}_I$  and under the constraint that the selected masks should not overlap, we formulate this problem as a K-shortest path search problem and detail our method below in Section B.1. Then, we detail in Section B.2 the second stage where we optimise the full objective function on the whole video while considering only the top combinations selected during the first stage.

### B.1. Image-Level Optimization

Given a frame  $I_t$ , we obtain a set of mask candidates  $\mathcal{M}_t$  using MP R-CNN. To identify the top- $K$  combinations of masks according to  $\mathcal{L}_I(I_t, \Delta_t)$  without having to perform an exhaustive evaluation, we iteratively apply Dijkstra’s algorithm [16]. To do this, we first construct a binary tree  $\mathcal{B}(\mathcal{V}, \mathcal{E})$ .

As shown in Figure 8 for the easy case where the masks in  $\mathcal{M}_t$  do not overlap, nodes  $\mathcal{V}_i = \{\mathcal{V}_{i,j}\}_j$  at the same level in the tree correspond to the state of the  $i$ -th mask  $M_{i,t} \in \mathcal{M}_t$  i.e. if it is selected or not, and edges  $\mathcal{E}_i = \{\mathcal{E}_{i,j}\}_j$  at the same level are weighted with the contribution to  $\mathcal{L}_I(I_t, \Delta_t)$  when mask  $M_{i,t}$  is selected or not. In this way, the problem of finding the most promising combinations of masks for a frame thus becomes to find the K-shortest paths in the binary tree  $\mathcal{B}(\mathcal{V}, \mathcal{E})$ .

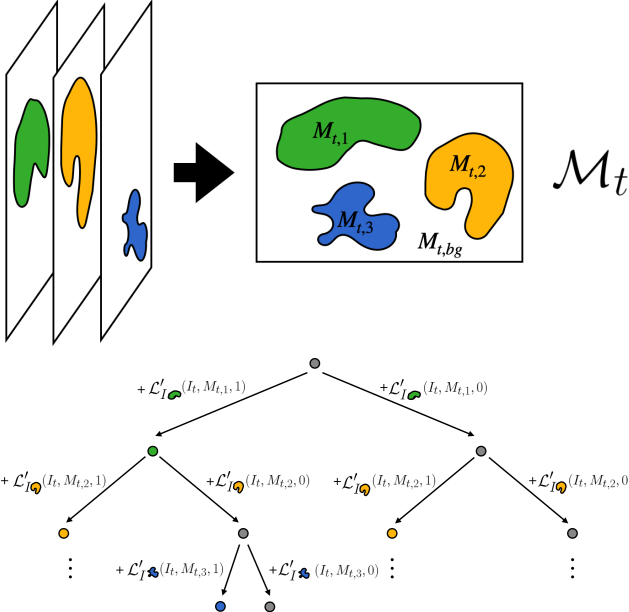


Figure 8. **Image-Level Optimization. Example of a tree  $\mathcal{B}(\mathcal{V}, \mathcal{E})$  in the non-overlapping case.** Nodes at the  $i$ -th level correspond to the selection ( $\delta_{t,i} = 1$ ) or non-selection ( $\delta_{t,i} = 0$ ) of the  $i$ -th mask. Edges at the  $i$ -th level are weighted according to the image term  $\mathcal{L}_I$  and depending whether or not the  $i$ -th mask is selected. As there is no overlaps among the three masks, the weights of edges can be calculated independently. A colored node corresponds to the selection of the mask with the same color; a gray node corresponds to the case where the mask is not selected.

The time complexity for finding these  $K$ -shortest paths by exhaustive search is  $O(2^N)$ , for  $N$  masks in each image, which is computationally prohibitive. We thus iteratively apply Dijkstra's algorithm [16] to efficiently find the top- $K$  shortest paths. We get the shortest path  $\mathcal{H}_1$  by directly applying Dijkstra's algorithm on the binary tree  $\mathcal{B}(\mathcal{V}, \mathcal{E})$ .

To find the next shortest path, we consider a set  $U$  of paths, initialized with  $\mathcal{H}_1$  as its only element. The whole procedure consists of two nested loops. The first loop is over each path  $\mathcal{H}$  in  $U$ . Given  $\mathcal{H}$ , the second loop is over each edge  $\mathcal{E}_{i,j}$  of  $\mathcal{H}$ . We set the weight of  $\mathcal{E}_{i,j}$  to infinity and apply Dijkstra's algorithm on the resulting tree. Each time we run Dijkstra's algorithm, we obtain an “intermediate shortest path” different from  $\mathcal{H}$ . After exiting the two loops, we add all the intermediate shortest paths to  $U$  and remove  $\mathcal{H}_1$  from it. The shortest path in  $U$  is now the second shortest path  $\mathcal{H}_2$  in the tree. We can then repeat the above procedure to get the next shortest paths.

This method decreases the time complexity from  $2^N$  to  $O(KN^3)$ , where  $N$  is the number of masks per image and  $K$  is the number of optimal combinations required.

Below, we start with the easier case, where there is no overlap among the mask candidates in  $\mathcal{M}_t$ . In this case,

each pixel in the image belongs to at most one mask candidate. The non-overlapping constraint is naturally satisfied, and the contributions of the masks to  $\mathcal{L}_I(I_t, \Delta_t)$  are independent of each other. Then, we dive into the overlapping case and show that we can transform the overlapping case to the non-overlapping case with a decomposing-then-hashing operation, and calculate  $\mathcal{L}_I(I_t, \Delta_t)$  exactly.

**Non-Overlapping Case.** We first consider the easier case where there is no overlap between the mask candidates, illustrated by Figure 8. In such case, image term  $\mathcal{L}_I(I_t, \Delta_t)$  can be written as a sum over the masks in  $\mathcal{M}_t$  plus a special additional mask made of the pixels that do not belong to any mask (recall that  $\Delta_t = \{\delta_{t,1}, \dots, \delta_{t,N}\}$ ):

$$\begin{aligned} \mathcal{L}_I(I_t, \Delta_t) &= \text{CE}(\text{Bg}(I_t), 1 - \bar{\text{Fg}}(\Delta_t)) \\ &= \sum_{M_{t,i} \in \mathcal{M}_t} \mathcal{L}'_I(I_t, M_{t,i}, \delta_{t,i}) + \bar{\mathcal{L}}_I(M_{t,bg}) \end{aligned} \quad (12)$$

with

$$\mathcal{L}'_I(I_t, M_{t,i}, \delta_{t,i}) = - \sum_{x \in M_{t,i}} (1 - \delta_{t,i}) \log \text{Bg}(I_t)(x) + \delta_{t,i} \log (1 - \text{Bg}(I_t)(x)), \quad (13)$$

where the sum is over image locations  $x$  in mask  $M_{t,i}$ , and

$$\bar{\mathcal{L}}_I(M_{t,bg}) = - \sum_{x \in M_{t,bg}} \log \text{Bg}(I_t)(x). \quad (14)$$

Term  $\bar{\mathcal{L}}_I(M_{t,bg})$  in Eq. (12) is constant.  $M_{t,bg}$  represents the background image generated for the selected masks. We can ignore it here for the selection of the top- $K$  mask combinations. Note that it still needs to be included in  $\mathcal{L}_I$  for the Video-Level Optimization. We can use the value of  $\mathcal{L}'_I(I_t, M_{t,i}, 1)$  as weight for an edge corresponding to the selection of mask  $M_{t,i}$ ,  $\mathcal{L}'_I(I_t, M_{t,i}, 0)$  as weight for an edge when mask  $M_{t,i}$  is not selected.

**Overlapping Case.** In general, the mask candidates predicted by MP R-CNN overlap, and the contributions of masks  $\{M_{t,i}\}_i$  to  $\mathcal{L}_I(I_t, \Delta_t)$  are no longer independent. We propose a decomposing-then-hashing method which first decomposes each mask into a group of non-overlapping sub-masks, then identify the contribution of each mask using the sum of the sub-masks. When adding a novel node to the path, we fit the non-overlapping constraint by inspecting if there are some sub-masks selected in both the current node and the nodes in this path.

As shown in Figure 9, we first decompose each mask  $M_{t,i}$  into a combination of sub-masks  $\{M'_{t,i,j}\}_j$  depending on whether the pixels in the mask belong to other masks or not. The whole image can thus be decomposed into the combination of all sub-masks  $\{M'_{t,i,j}\}_{i,j}$  and  $M_{t,bg}$ , with no overlaps among the sub-masks in  $\{M'_{t,i,j}\}_{i,j}$ . Then, we can construct a hash table where the key is the index of each

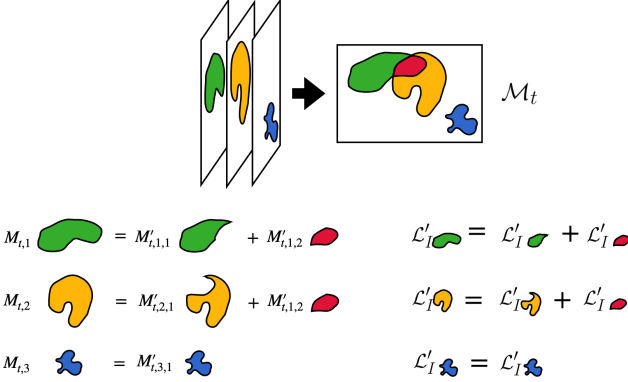


Figure 9. **Image-Level Optimization. Decomposing-the-hashing for the overlapping case.** The red mask represents the overlapping region between  $M_{t,1}$  and  $M_{t,2}$ . The contribution of  $M_{1,t}$  can thus be decomposed into the sum of contributions of the two non-overlapping green and red sub-masks.

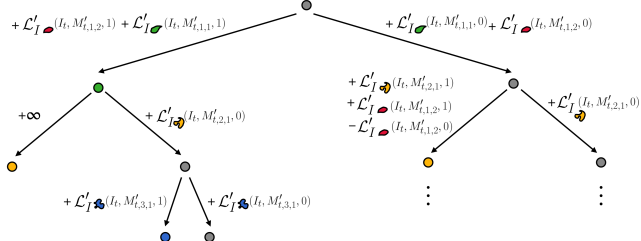


Figure 10. **Image-Level Optimization. Example of  $\mathcal{B}(\mathcal{V}, \mathcal{E})$  in the overlapping case.** Each time a node is added in the path, the weight of the edge is calculated by considering all the previous nodes in the path.

mask  $M_{t,i}$  and the value is the index of corresponding sub-masks  $\{M'_{t,i,j}\}_j$  for each mask  $M_{t,i}$ .

Similar to the non-overlapping case, with the help of non-overlapping sub-masks, we have:

$$\begin{aligned} \mathcal{L}'_I(I_t, M_{t,i}, \delta_{t,i}) = & - \sum_{S \in \{M'_{t,i,j}\}_{i,j}} \sum_{x \in S} \left( (1 - \delta_{t,i}) \log \text{Bg}(I_t)(x) + \right. \\ & \left. \delta_{t,i} \log (1 - \text{Bg}(I_t)(x)) \right) \end{aligned} \quad (15)$$

which means that the contribution of each mask to  $\mathcal{L}_I(I_t, \Delta_t)$  can be decomposed into the sum of the contributions of its corresponding sub-masks. Eq. (12) can thus be written as:

$$\mathcal{L}_I(I_t, \Delta_t) = \sum_{S \in \{M'_{t,i,j}\}_{i,j}} \mathcal{L}'_I(I_t, S) + \bar{\mathcal{L}}_I(M_{t,bg}). \quad (16)$$

A tree for an overlapping case is shown in Figure 10. When searching for the shortest path in the graph, given a path, each time a node is added to the path, with the help of the hash table constructed aforementioned, we first check whether there are any sub-masks  $M'_{t,i,j}$  already being assigned a certain “state” in the previous nodes (by state, we

mean if it has been selected as foreground or selected as background).

If not, like the non-overlapping case, we consider the  $\mathcal{L}'_I(I_t, M_{t,i}, \delta_{t,i})$  for the weight of the edge  $B$ ,  $\forall i > 0$ .

If a sub-mask has already been assigned some state, there are two possible cases. The first case is that the sub-masks  $M'_{t,i,j}$  selected both in the current node and a previous node have the same state. When the state is “background”, as we have already counted the contribution of sub-masks in previous edges, the weight of the current edge is assigned to the sum of the contribution of the rest of masks. When the state is “foreground”, since the masks should not overlap, the weight of the current edge is set to infinity to prohibit this path from becoming one of the top- $K$  shortest paths. The second case is that some sub-masks  $M'_{t,i,j}$  selected both in the current node and a previous node possess different states. In order to calculate the weight of the current edge, along with the contribution of each sub-mask by considering the state assigned by the current node, we subtract the contribution of the shared sub-masks according to their assigned state in the previous node.

## B.2. Video-Level Optimization

As shown in Figure 11, after the top- $K$  combinations of masks for each frame have been found by the first stage, we construct a graph  $\mathcal{G}(\mathcal{V}, \mathcal{E})$  to find the best combinations of masks for each frame by optimizing the objective function over the whole video. Node  $\mathcal{V}_{t,k}$  represents the  $k$ -th combination of masks of frame  $I_t$ .  $\mathcal{E}_{t,t+1,k,k'}$  represents the edge that connects node  $\mathcal{V}_{t,k}$  and node  $\mathcal{V}_{t+1,k'}$ . The weight of edge is a sum over the image term, the flow term and the motion model term:

$$\begin{aligned} \text{Weight}_{\mathcal{E}_{t,t+1,k,k'}} = & \lambda_I \mathcal{L}_I(I_t, \Delta_t) + \\ & \lambda_F \mathcal{L}_F(F_t, I_t, I_{t+1}, \Delta_t, \Delta_{t+1}) + \\ & \lambda_p \mathcal{L}_p(\Delta_t, \Delta_{t+1}). \end{aligned} \quad (17)$$

In our case, as the weight of every edge is non-negative, we can use Dijkstra’s algorithm [16] to select the combination of masks among the top- $K$  combinations for each frame.

## C. Generation of Synthetic Flow $\bar{F}_t$

The motion of the selected objects should be consistent with the optical flow. To deal with camera motion, we consider that the optical flow of the background can be different from 0 (but uniform). Given two consecutive frames  $I_t$  and  $I_{t+1}$ , together with two combinations of masks  $\Delta_t$  and  $\Delta_{t+1}$  for these frames, we propose a method to generate a “synthetic optical flow” which is then compared against the optical flow predicted by some optical flow model.

An overview of the generation pipeline is shown in Figure 12. We first generate two synthetic images  $I'_t$  and  $I'_{t+1}$

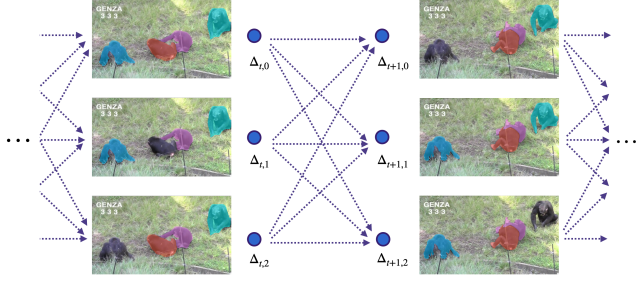


Figure 11. **Video-Level Optimization.** Example of graph  $\mathcal{G}(\mathcal{V}, \mathcal{E})$ , represented only between two consecutive frames  $I_t$  and  $I_{t+1}$  for a video sequence of chimpanzees. Each image in the column represents a combination of masks  $\Delta_t$ , different masks are shown in different colors (Best seen in color).

by cropping and pasting the content of selected masks in frame  $I_t$  and  $I_{t+1}$  to a background image  $I_{bg}$  randomly selected from the Internet. Then we pass the pair of synthetic images into a optical flow model  $g$  to generate a synthetic  $\bar{F}_t$ . The pixels outside the selected masks are assigned the average flow in  $F_t$  computed over the background.

The motivation for using a background image rather than a uniform background color which seems more natural is to make sure the objects are visible before computing the flow. For example, in the case of Figure 11, using a uniform black background would make optical flow prediction fail for the dark chimpanzees. Using a real image is a simple way to prevent this problem.

## D. Implementation Details

### D.1. Training Details

All our experiments were carried out on 4 Nvidia RTX 2080Ti GPUs. During the training, mixed precision training is used to reduce memory consumption and accelerate training.

**Pre-training.** For the pre-training on the COCO dataset, we use the open source repo of Mask-RCNN [43] and follow the training setting of [23], except that we adopt the class-agnostic setting, where all 80 classes are merged into a single “object” category. We use ResNet-50-FPN [38] as our backbone. As in [49], we call the Mask R-CNN model trained using this class-agnostic setting “MP R-CNN” for Mask Proposal R-CNN. Our backbone network is initialized with weights pre-trained on ImageNet [14]. During training, the shorter edge of images are resized to 800 pixels. Each GPU has 4 images and each image has 512 sampled RoIs, with a ratio of 1:3 of positives to negatives. We train our Mask R-CNN for 90k iterations. The learning rate is set to 0.02 at the beginning and is decreased by 10 at the 60k and 80k iteration. We use a weight decay of 0.0001 and momentum of 0.9.

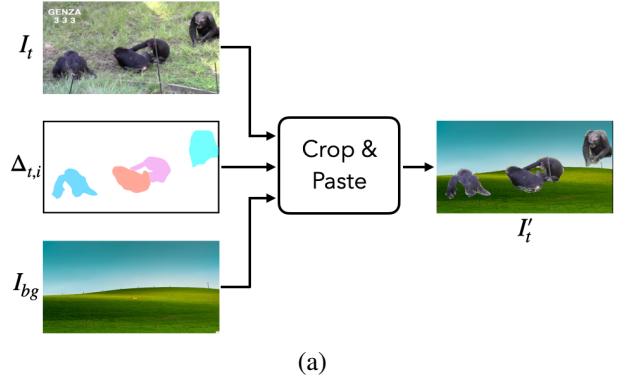


Figure 12. **Generation pipeline for “synthetic optical flow”**  $\bar{F}_t$ . (a) We first generate two synthetic images  $I'_t$  and  $I'_{t+1}$  by cropping and pasting the content of selected masks in frame  $I_t$  and  $I_{t+1}$  to a background image  $I_{bg}$  randomly selected from the Internet. (b) We then feed the pair of synthetic images to a optical flow model  $g$  to generate a synthetic  $\bar{F}'_t$ . (c) The pixels outside the selected masks are assigned the average flow in  $F_t$  computed over the background.

**Fine-tuning.** We finetune MP R-CNN on the masks of Unseen-VIS-train generated by our method for 1k iterations. The initial learning rate is set to 0.002. The rest of the parameters and data augmentation strategies are set to be the same with the parameters used for pre-training. For the *DAVIS Unsupervised* benchmark, we finetune MP R-CNN on the masks generated on the 60 training videos

Pretrained on COCO	Unseen-VIS-train		Training Strategy	Unseen-VIS-test					COCO val						
	GT	Generated Masks		AP	AP <sub>50</sub>	AP <sub>75</sub>	AR <sub>1</sub>	AR <sub>3</sub>	AR <sub>5</sub>	AP	AP <sub>50</sub>	AP <sub>75</sub>	AP <sub>S</sub>	AP <sub>M</sub>	AP <sub>L</sub>
✓			—	35.8	61.2	38.1	33.3	47.3	50.3	35.3	62.6	35.9	20.8	40.6	52.4
✓		✓	retrain	51.2	80.2	56.8	45.0	56.8	59.5	34.9	61.8	35.7	20.6	40.2	52.3
✓		✓	retrain	38.9	67.8	41.2	35.2	48.9	51.4	35.0	62.0	35.8	20.5	40.2	52.3
✓	✓		finetune	50.8	80.9	54.6	43.6	58.6	60.6	24.0	44.9	23.4	15.3	28.7	33.6
✓	✓	✓	finetune	39.0	67.9	41.3	35.2	48.9	51.4	32.1	57.0	32.8	17.5	39.3	51.1

Table 5. Results on the COCO2017 validation dataset and Unseen-VIS-test adopting different training strategies. The performance of MP R-CNN fine-tuned on our generated masks on Unseen-VIS-train is much less affected compared to MP R-CNN fine-tuned on the ground truth masks. By training on the dataset created by naively mixing the training dataset of COCO with our generated masks on Unseen-VIS-train, we can achieve the same results on Unseen classes as fine-tuning while preserving the performance on Seen classes.

of DAVIS2017 dataset, using the same hyper-parameters as for Unseen-VIS-train.

## D.2. Implementation Details for the Related Methods

### D.2.1 Foreground/Background Segmentation

In order to estimate the background regions present in the image, similar to [32], we adopt a FPN based network for segmentation. We use ResNest-200 [75] as our backbone. The regions that contain instances are considered as foreground and background otherwise to generate binary mask for training. We set the initial learning rate to 0.02, then decrease it by 10 at the 240k and 255k iteration. The batch size is set to 16. Scale augmentation is applied during training to further improves results.

### D.2.2 Optical Flow Estimation

We use the model released by [58] trained on FlyingThings [44]. FlyingThings is a large-scale synthetic dataset for optical flow estimation. The dataset is generated by randomizing the movement of the camera and synthetic objects collected from the ShapeNet dataset [7]. The model for optical flow estimation is pre-trained on FlyingThings for 100k iterations with a batch size of 12, then for 100k iterations on FlyingThings3D with a batch size of 6.

### D.2.3 Video Object Segmentation

**NLC [18].** We use the re-implementation code provided by [51]. In the original implementation of the NLC algorithm, an edge detector pre-trained on labeled edge images [17] is used, while the re-implementation of [51] replaces the trained edge detector with unsupervised superpixels. In order to obtain a motion segmentation for each frame, a per-frame saliency map based on motion is computed then averaged over superpixels calculated using method from [1]. Meanwhile, a nearest neighbor graph is computed over the superpixels in the video using location and appearance as features. Finally, the saliency is propagated across frames using a nearest neighbor voting scheme. For more details, please refer to [18, 51].

**FST [50].** We use the official code released by the authors to generate masks on the videos from Unseen-VIS-train.

**IOA [12].** We use the official code released by the authors. We first use the official code of the VideoPCA algorithm [57] to find the saliency regions which stand out the background in terms of motion and appearance. Then we follow the same approach as in [12] to keep only the top 20% saliency maps based on the mean score of the non-zero pixels. The remaining saliency maps are used for training of the PSPNet [76] with ResNet-50 [24] as backbone, and initialized with ImageNet pre-trained weights [14].

**UnOVOST [41].** We use the official code released by the authors, and use our MP R-CNN for mask proposals generation. All the hyper-parameters are kept the same as in the original work [41].

**TWB [3].** We use the official code released by the authors, and replace the human detector with our MP R-CNN. Since the confidence score for objects of unseen classes are sometimes low, we lower the thresholds for filtering detection proposals and regression results to 0.1. Note that [3] applies a Re-ID network to re-identify the persons that are missing in previous frames, in order to re-identify the animals in Unseen-VIS-train, we replace the Re-ID network trained on the pedestrian dataset with a ResNet-50 pre-trained on ImageNet [14].

**Data Distillation [55].** We use the official code released in Detectron2 [67] and follow the same pipeline as stated in [55] for filtering and retraining.

**UVC [36].** We use the model released by the authors for mask wrapping. The model is trained in a self-supervised manner on the Kinetics [31] dataset. During inference, we follow the same setting of UVC to resize the shorter edge of image to 480 pixels. For Zero-Shot UVC, the masks for the first frame are obtained by selecting the masks predicted

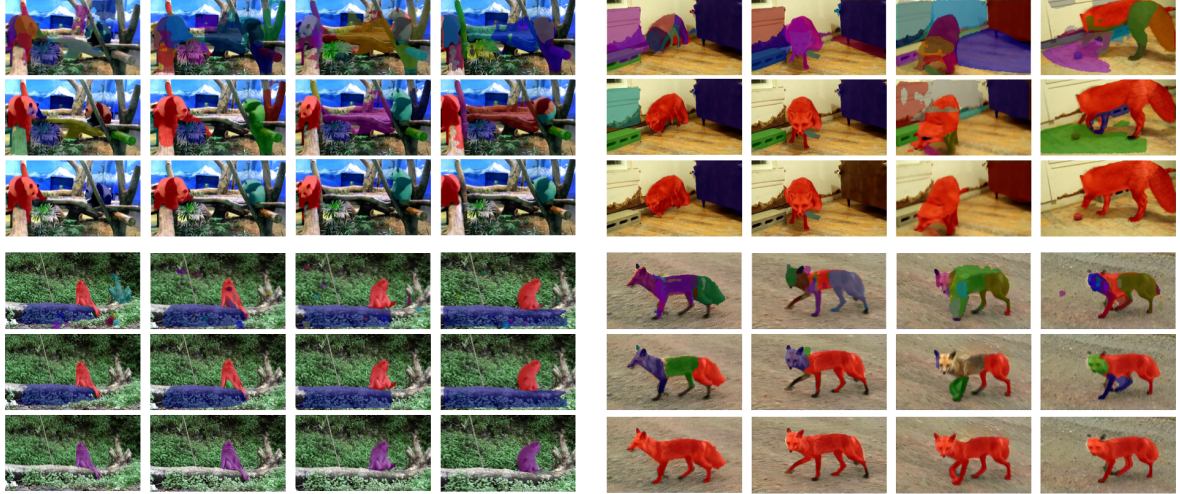


Figure 13. **Qualitative results for the mask selection by UnOVOST and by our approach on new classes.** We show in this figure masks extracted from a sequence (from Unseen-VIS-train). First row and fourth row: Masks detected by baseline network MP R-CNN; Second row and fifth row: Masks selected by UnOVOST [41]; Third row and sixth row: Masks selected by our approach. Our method chooses the correct masks among the raw detections, while UnOVOST makes several mistakes. *For more examples, please refer to the video.*

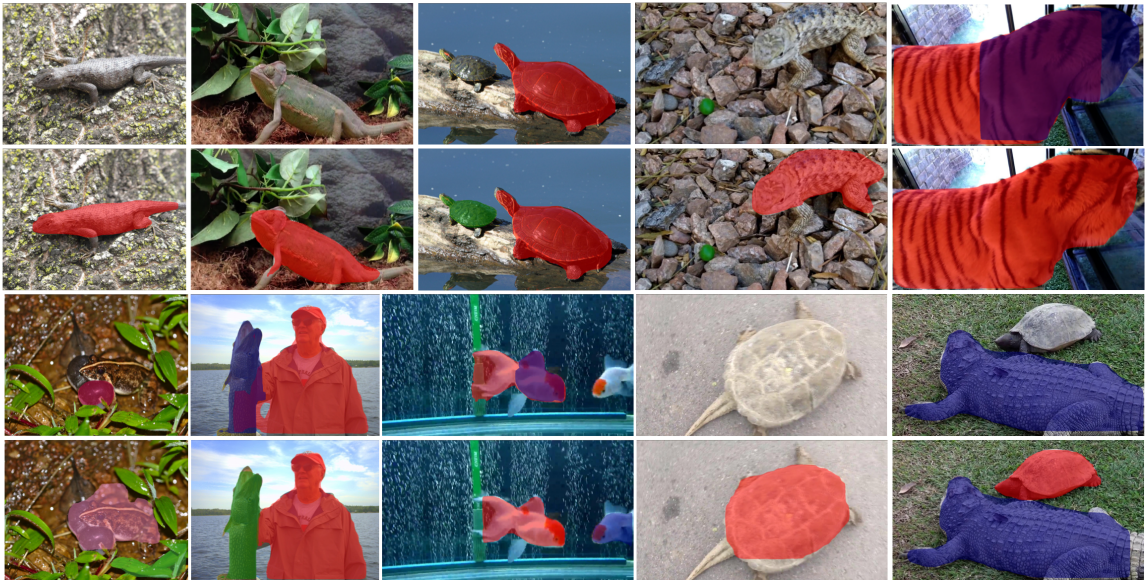


Figure 14. **Qualitative results for detected masks of new classes, before and after fine-tuning on our generated masks.** We show in this figure masks detected in *still images*. First row and third row: Detections by MP R-CNN before fine-tuning; Second row and fourth row: Detections by MP R-CNN after fine-tuning on our selected masks; The masks generated by our method results in a significantly better model for the new classes. *For more examples, please refer to the video.*

by MP-RCNN on the first frame whose confidence score is larger than 0.1.

**RVOS [60].** We use the official code released by the authors, and replace the backbone of RVOS by ResNet-50. Input images are resized to  $256 \times 448$ . Each batch is composed with 4 clips of 5 consecutive frames. The model is trained on the 1089 videos of seen classes on YouTube VIS [71] for

50 epochs. The Adam optimizer is used to train our network and the initial learning rate is set to  $1e-6$ .

## E. Results on COCO dataset

Detailed results are shown in Table 5. The performance of MP R-CNN on COCO-2017-val degrades dramatically after finetuning on either the ground truth of Unseen-VIS-train or the masks generated by our approach. Our guess

is that this degradation results from the significant domain gap between images in YouTube-VIS and COCO. Interestingly, compared with the ground truth of Unseen-VIS-train, the performance of MP R-CNN is much less affected by finetuning on the masks generated by our approach, which demonstrates that our approach helps to preserve to some extent the information of the dataset used for pre-training.

For retraining, we use a naive strategy to train MP R-CNN from scratch on the mixture of COCO dataset and labels from Unseen-VIS-train. We add the images and annotations of Unseen-VIS-train into the COCO dataset, the annotations can be either ground truth or masks generated with our approach. Then we follow the training strategy given in Section D.1. Mask R-CNN is trained on 120k training images of COCO for 90k iterations with batch size 16. The mixture of COCO and Unseen-VIS-train has 20k additional training images from Unseen-VIS-train, we thus train the our MP R-CNN on the mixture dataset for 110k iterations.